

Semiconductor laser with phase-conjugate feedback: Dynamics and bifurcations

Bernd Krauskopf,^{1,*} George R. Gray,² and Daan Lenstra¹

¹*Faculteit Natuurkunde en Sterrenkunde, Vrije Universiteit, De Boelelaan 1081, 1081 HV Amsterdam, The Netherlands*

²*Seagate Technology, Riverbluff Development Center, 10701 Lyndale Avenue South, Bloomington, Minnesota 55420*

(Received 30 March 1998; revised manuscript received 12 August 1998)

This paper presents the dynamics and bifurcations of a semiconductor laser subject to instantaneous phase-conjugate feedback. Recently, the behavior of such a laser has been explored by means of bifurcation diagrams. However, the exact nature of the involved dynamics and bifurcations remained unclear. Here we present a detailed study of the changes of the dynamics as the feedback strength is varied. Most prominent are symmetry-breaking and -restoring bifurcations, tori and their bifurcations, and a sudden transition between chaos and a stable limit cycle due to a saddle-node bifurcation of limit cycles. [S1063-651X(98)01812-1]

PACS number(s): 05.45.+b, 42.65.Sf

I. INTRODUCTION

There has been considerable interest recently in the coupling of semiconductor lasers to phase-conjugate mirrors (PCMs) due to potential practical applications as well as to the interesting resulting dynamics [1–10]. On the practical side, such a laser with phase-conjugate feedback (PCF) can be used for mode locking [1], phase locking [2–4], and frequency control [5,6]. PCF can lead to very complex dynamics, which seems to be partly because PCF can be considered a combination of regular feedback (because of the delay) and injection (because of the presence of detuning). A comparison of PCF with regular feedback has recently been conducted [4]. This comparison, however, was performed with the aid of bifurcation diagrams, without exploring in detail the underlying dynamics.

In this paper we explore the complex dynamical behavior of a single-mode semiconductor laser subject to weak instantaneous PCF. The main chain of events as the feedback strength is increased can be sketched as follows. When the laser is detuned slightly from the PCM, the solitary-laser solution becomes unstable and then phase locking occurs, in which the laser locks to the phase generated by the phase-conjugate mirror. The locked solution undergoes a Hopf bifurcation generating a stable limit cycle that corresponds to periodic changes in the power, the so-called relaxation oscillations. In the bifurcation diagram one finds intervals with stable limit cycles, interspersed with intervals, which we call *bubbles*, with more complicated dynamics (Fig. 1). The transition from one stable limit cycle to the next differs from bubble to bubble. In bubble 1 we find a transition to chaos via period doublings. In other bubbles there is a transition to chaos via motion on an invariant torus (with quasiperiodic or phase-locked dynamics). We also find a sudden transition between chaos and a limit cycle via a saddle-node bifurcation of limit cycles. Finally, symmetry-breaking and symmetry-restoring bifurcations are prominent features of the dynamics.

Our main point here is that one is likely to miss important phenomena if one just considers a bifurcation diagram. This is why we show the behavior of the laser for a single value of the feedback strength in different ways: by a time series of the power, by an optical spectrum, by a (two-dimensional projection of a) trajectory, and by the respective attractor of the Poincaré map. By comparing these representations for different values of the feedback strength, one can get a very detailed picture of the bifurcations, that is, of the qualitative changes of the dynamics. The optical spectra also predict how the dynamics and the bifurcations could be most easily identified in an experiment.

The paper is organized as follows. In Sec. II we describe the model, and in Sec. III we explain the bifurcation diagram, which serves as our starting point. In Sec. IV we look in detail at the laser dynamics. Section V discusses the implications of bifurcations involving the symmetry, and Sec. VI explains the sudden transition to chaos. We draw general conclusions and summarize in Sec. VII.

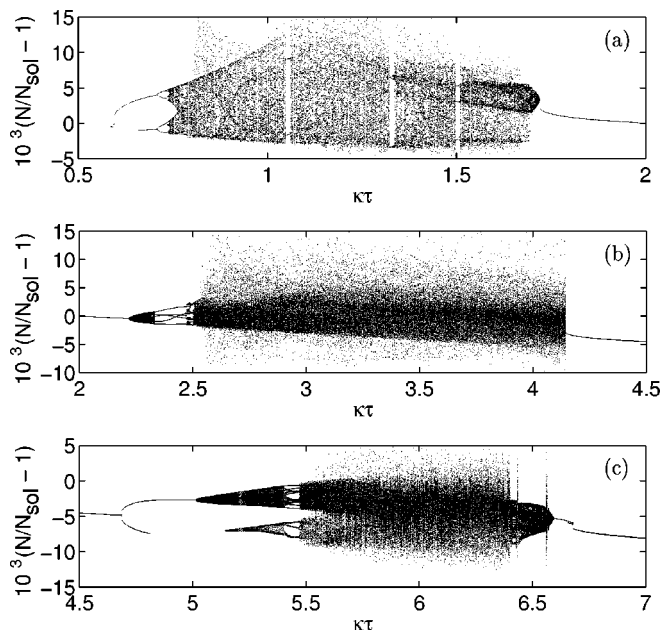


FIG. 1. The bifurcation diagram for $\kappa\tau \in [0.5, 7]$, showing normalized inversion when the power crosses its average, consists of three bubbles.

*Present address: Department of Engineering Mathematics, University of Bristol, Bristol BS8 1TR, U.K. Electronic address: B.Krauskopf@bristol.ac.uk

II. SINGLE-MODE RATE EQUATIONS WITH PCF

We assume that a single-mode semiconductor laser is obtaining weak feedback from a PCM which responds instantaneously. The assumption of weak PCF allows us to include only a single round-trip in the external cavity. The assumption of a very fast PCM allows us to ignore the dynamics of the mirror itself. In fact, it was recently shown [11–13] that even the interaction time within the PCM must be taken into account for an accurate treatment of the laser dynamics. However, for short interaction times, the exact treatment reduces to that of the instantaneous mirror. The interaction time can in fact be controlled by the PCM pump power [11].

The theoretical model for this paper is described by the following rate equations for the slowly varying complex amplitude of the intracavity optical field $E(t)$ and for the inversion $N(t)$:

$$\frac{dE}{dt} = \frac{1}{2} \left[-i\alpha G_N [N(t) - N_{\text{sol}}] + \left(G - \frac{1}{\tau_p} \right) \right] E(t) + \kappa E^*(t - \tau) \exp[2i\delta(t - \tau/2)], \quad (1a)$$

$$\frac{dN}{dt} = \frac{I}{q} - \frac{N(t)}{\tau_e} - G|E(t)|^2. \quad (1b)$$

In these equations $|E(t)|^2$ is the photon number. To convert to the power, there are 1.71×10^4 photons per mW. Furthermore, α is the linewidth-enhancement factor, G_N is related to the derivative of the optical gain, N is the electron population, N_{sol} is its steady-state value in the absence of feedback, G is the net rate of stimulated emission, τ_p is the photon lifetime, I is the injection current, q is the magnitude of the electron charge, and τ_e is the electron lifetime. The stimulated emission term G includes the effect of nonlinear gain, that is, $G = G_L(1 - \epsilon P)$, where $G_L = G_N(N - N_0)$ is the linear gain and ϵ is the nonlinear-gain coefficient. Here N_0 is the transparency electron number, which is related to N_{sol} by $N_{\text{sol}} = N_0 + G_N/\tau_p$. The last term in Eq. (1a) models the phase-conjugate feedback, and it contains three parameters: the feedback rate κ , the detuning δ , and the external-cavity round-trip time τ . They are given by

$$\kappa = \frac{(1 - R_m)}{\tau_L} \left[\frac{\eta_c R_{\text{ext}}}{R_m} \right]^{1/2} \quad \text{and} \quad \tau = \frac{2L_{\text{ext}}}{c}, \quad (2)$$

where R_m is the laser front-facet reflectivity, τ_L is the round-trip time in the solitary laser cavity, η_c is the coupling efficiency and is taken to be unity due to the self-aligning nature of the PCM, R_{ext} is the power reflectivity of the PCM, and L_{ext} is the distance between the laser and the PCM.

Note that the field which is fed back to the laser has been conjugated by the PCM. Spontaneous-emission Langevin-noise terms are intentionally left off in Eqs. (1a) and (1b), since we want to consider only deterministic effects in this paper. We also neglect multiple feedback terms for Eq. (1a) due to the assumption of weak feedback. The numerical values of the parameters used in the model were chosen to model a typical laser used for writing to optical disks. Throughout all computations we used

$$\alpha = 3, \quad G_N = 1190 \text{ s}^{-1}, \quad N_0 = 1.64 \times 10^8,$$

$$\epsilon = 3.57 \times 10^{-8}, \quad I = 65.1 \text{ mA},$$

$$\tau_p = 1.4 \text{ ps}, \quad \tau_e = 2 \text{ ns}, \quad R_m = 0.12,$$

$$\tau_L = 9.3 \text{ ps}, \quad \text{and} \quad L_{\text{ext}} = 10 \text{ cm}.$$

These values lead to a threshold current of 61.9 mA. Also, because of the presence of nonlinear gain, there is an effective detuning of $\delta = 166$ MHz. Finding the numerical values of these parameters in practice is hard, but good estimates can be found by making a number of key experimental measurements [14].

From a dynamical systems point of view, Eqs. (1a) and (1b) are a three-dimensional delay-differential system [15,16]. These equations describe how a function defined on the interval $[-\tau, 0]$ (the initial condition) with values in \mathbb{R}^3 [the (E, N) space] evolves in the time interval $[0, \tau]$ and so on for all future (positive) values of time. The interval $[0, \tau]$ can be shifted back to $[-\tau, 0]$, so that Eqs. (1a) and (1b) define an operator on the infinite-dimensional space of functions over $[-\tau, 0]$ with values in (E, N) space. Here we adopt the common and probably most physical way of thinking about Eqs. (1a) and (1b), namely, we simply consider the time evolution $(E(t), N(t))$ in the three-dimensional (E, N) space of a given initial condition, specified by the values of $(E(t), N(t))$ on $[-\tau, 0]$. [Mathematically speaking, this is a projection of the infinite-dimensional dynamics onto (E, N) space.] This is particularly useful once the system has settled down to an attractor.

An important feature of Eqs. (1a) and (1b) is their symmetry with respect to the transformation $E \mapsto -E$, which is a rotation by π of the E plane. As a consequence, any attractor we find will be either symmetric, or have a symmetric counterpart, which can be found by changing the phase of an appropriate initial condition by π . This symmetry also allows for the possibility of symmetry-breaking and -restoring bifurcations. As general references to the aspects of symmetry in dynamical systems see Refs. [17,18]. In symmetry breaking, a symmetric attractor becomes unstable, creating two nonsymmetric attractors, which are mapped to each other by the transformation $E \mapsto -E$. In symmetry restoration, two nonsymmetric attractors grow in size, collide, and give rise to a symmetric attractor. We refer to Sec. IV for examples of these bifurcations, and to Sec. V for their physical implications.

III. THE BIFURCATION DIAGRAM

A first impression of the dynamics and the bifurcations of the laser in the presence of PCF can be obtained by a bifurcation diagram, in which a key quantity is plotted against the main (dimensionless) parameter $\kappa\tau$; see, for example, [4,10,11]. However, the bifurcation diagrams in the literature are quite crude, and they do not make it clear what the actual dynamics are and how they depend on $\kappa\tau$.

As a starting point for our study we consider the bifurcation diagram in much higher resolution in three pieces in Fig. 1. It has been obtained as in Ref. [11] in the following way: after allowing transients to die away, the normalized value $[10^3(N/N_{\text{sol}} - 1)]$ is recorded whenever the power crosses

its average value (over the orbit) P_{ave} in the increasing direction. This procedure is repeated for increasing PCF strength, that is, for increasing $\kappa\tau \in [0.5, 7]$. Each time we increase or decrease the PCF strength, the laser variables retain their final values from the previous PCF strength as initial condition, just as would be the case in an experiment. We stress that there is no hysteresis: computing the bifurcation diagram by decreasing $\kappa\tau$ gives the same result. In other words, for any $\kappa\tau$ there is exactly one attractor (up to symmetry; see Sec. V), which is very different from the situation for conventional optical feedback [9].

The interpretation of the bifurcation diagram is as follows. For a given feedback strength, the absence of points in the diagram indicates a stable equilibrium solution (e.g., $\kappa\tau = 0.5$). A small number of points for a given $\kappa\tau$ corresponds to a periodic limit-cycle solution (e.g., $\kappa\tau = 2.0$). Finally, a large number of points corresponds to quasiperiodicity or chaos (e.g., $\kappa\tau = 3.0$). One can clearly see three *bubbles* with more complicated dynamics.

It is the purpose of this paper to study the dynamics and bifurcations in great detail. To this end we will give a careful analysis of how the dynamics in (E, N) space depend on $\kappa\tau$. We will concentrate on the study of the first three bubbles, for $\kappa\tau \in [0.5, 7]$, by means of simulation. This will explain many features in the bifurcation diagram in Fig. 1, which remain somewhat mysterious at this point. We argue that it is practically impossible to interpret all features of the bifurcation diagram without good knowledge of the dynamics in (E, N) space.

IV. DESCRIPTION OF THE DYNAMICS

In this section we take a dynamical systems point of view and describe the bifurcations as we pass through bubbles 1, 2, and 3 when $\kappa\tau$ is increased from 0.5 to 7.0. As general references to bifurcation theory see [19,20]. In order to give the reader a good idea of the dynamics and the bifurcations, we present them in several ways. For each bubble we consider the dynamics for a representative set of $\kappa\tau$ values and collect them in one main figure. For each value of $\kappa\tau$ we show (in three panels) the time series of the power (left panel, units are ns and mW), the optical spectrum (middle panel, units are GHz and arbitrary units), and the orbit projected onto the E plane (right panel, the units are such that $|E|^2$ is the photon number). In a separate figure we show the respective attractors of the Poincaré map, given by the intersections of the attractor in (E, N) space with the Poincaré plane $N = N_{\text{ave}}$. This means that a limit cycle results in a discrete set of points, quasiperiodic motion on a torus results in a circle, and chaotic motion results in a complicated set in the Poincaré plane. For pictures of the dynamics in (E, N) space and for RIN spectra see Refs. [21,22].

The data have been obtained as follows. With the initial condition $(E(t), N(t)) = 0$ for all $t \in [-\tau, 0]$ Eqs. (1a) and (1b) were integrated on the computer using a fourth-order Runge-Kutta algorithm. Note that this initial condition corresponds to first blocking the path to the PCM in an experiment. The integration time step was generally 8 ps, but was regularly reduced to ensure the accuracy of the algorithm. In order to allow for transient behavior to die off, we discarded the data for the initial 1000 ns. For calculation of the optical

spectra, 4096 points were used with 32 ps between points, so that the resolution in the frequency domain is 7.63 MHz. Each spectrum shown represents an average over ten spectra, to improve the signal-to-noise ratio. Further, we have plotted the optical spectra on a logarithmic vertical scale, so that the widely varying magnitudes of the peaks show up better.

A. Outside the bubbles

In contrast with conventional optical feedback, PCF immediately destabilizes the laser power even for extremely low feedback strengths. For example, $\kappa\tau = 0.01$ already produces a limit cycle with oscillation frequency of 320 MHz. Such a low value of feedback corresponds to an effective PCM power reflectivity of $R_{\text{ext}} = -85$ dB. The 320 MHz frequency is about twice the detuning between the PCM pump laser and the solitary laser frequency. Such a detuning obviously does not exist in ordinary optical feedback. The origin of the oscillations is the beating between the pump laser and the solitary laser. As the feedback level increases beyond $\kappa\tau = 0.01$, the feedback induces a frequency shift which attempts to cancel the pump detuning. In other words, the PCF is pulling the laser frequency toward the pump frequency [4] until locking occurs at $\kappa\tau \approx 0.222$.

Although locking to an external-cavity frequency can occur with ordinary feedback, the frequency locking occurring here is accompanied by phase locking as well, so that the laser phase no longer undergoes diffusion [2,3]. Since phase diffusion is responsible for the laser linewidth, the phase locking found here manifests itself in an ultranarrow laser linewidth; the linewidth becomes limited by the linewidth of the pump laser. Simulations have shown that this narrow linewidth state is stable even when the spontaneous-emission noise terms are turned on [4].

The next destabilization occurs as the feedback reaches $\kappa\tau \approx 0.59$, which marks the edge of the locking band [Fig. 1(a)]. A Hopf bifurcation occurs corresponding to the undamping of the relaxation oscillations, which leads to a stable limit cycle in (E, N) space. The attracting limit cycle is not symmetric and, consequently, its symmetric counterpart is a second attractor. When $\kappa\tau$ is increased further, bubble 1 is entered.

Although occasional locking is seen inside the bubbles, between the bubbles the laser is always frequency locked, although not phase locked, with the power oscillating close to some multiple of the fundamental external-cavity frequency $1/\tau = 1.5$ GHz. Thus for $\kappa\tau \approx 2.0$, $\kappa\tau \approx 4.2$, and $\kappa\tau \approx 7.0$, the frequency of the limit cycle is approximately 1.5 GHz, 3 GHz, and 4.5 GHz, respectively. An explanation for the width of these locking regions was recently derived [11].

B. Transition through bubble 1

The chain of events is depicted in Fig. 2 and the associated attractors of the Poincaré map can be found in Fig. 3; compare also Fig. 1(a). The stable limit cycle, corresponding to the relaxation oscillation, undergoes a sequence of period-doubling bifurcations until a chaotic attractor is created [Figs. 2(a)–2(c) and 3(a)–3(c)]. When $\kappa\tau$ is increased further, the chaotic attractor grows until it collides with its symmetric counterpart ($\kappa\tau = 0.8$), which is responsible for clearly visible excursions into the region where $\text{Re}(E) < 0$ in

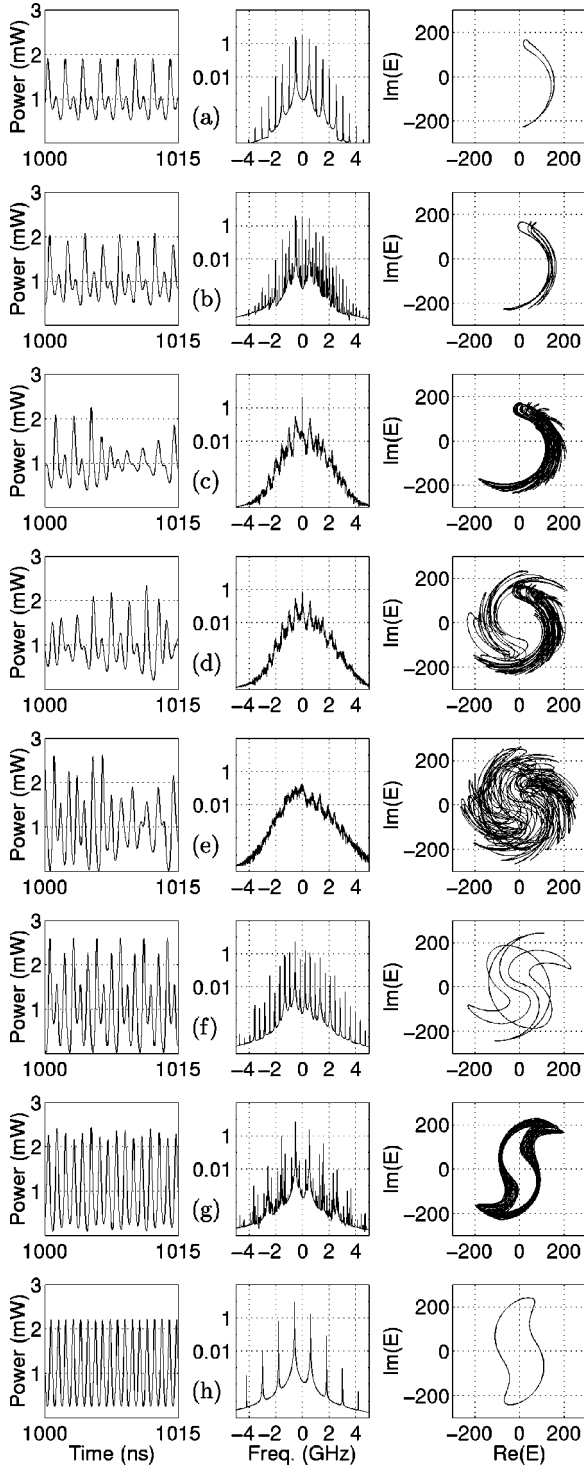


FIG. 2. Transition through bubble 1, showing the time series of the power (left panel), the optical spectrum (middle panel), and the trajectory in the E plane (right panel). From (a) to (h) $\kappa\tau = 0.7, 0.735, 0.79, 0.8, 1.45, 1.5, 1.71,$ and 1.75 .

Figs. 2(d) and 3(d). This is a symmetry-restoring bifurcation, and the attractor is symmetric through the remainder of bubble 1. The chaotic regime [$\kappa\tau = 1.45$, Figs. 2(e) and 3(e)] is interspersed with windows of periodic orbits in the region of chaos, for example, near $\kappa\tau = 1.5$ [Figs. 2(f) and 3(f)]. The end of the chaotic region is marked by the appearance of motion on a torus, which appears to be quasiperiodic [Figs. 2(g) and 3(g)]. The torus becomes smoother and rounder

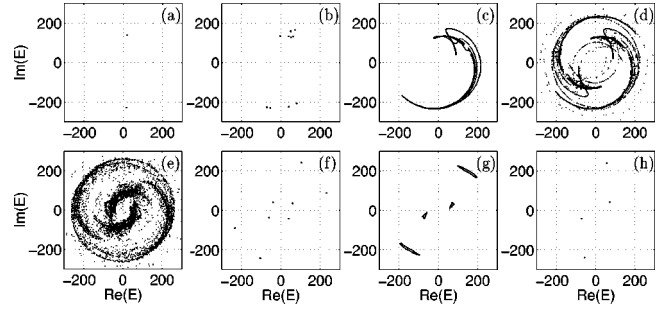


FIG. 3. Attractors of the Poincaré map of the transition through bubble 1 for the values of $\kappa\tau$ in Fig. 2.

while it shrinks in size, and it finally disappears in a Hopf bifurcation of the Poincaré map. After this, we leave bubble 1 and are left with a symmetric limit cycle [Figs. 2(h) and 3(h)].

C. Transition through bubble 2

The transition through bubble 2 is depicted in Figs. 4 and 5; compare also Fig. 1(b). When bubble 2 is entered, the Poincaré map undergoes a Hopf bifurcation, so that the stable limit cycle bifurcates to a torus. The motion on the torus may be quasiperiodic ($\kappa\tau = 2.3$) or locked ($\kappa\tau = 2.45$); see Figs. 4(a)–4(d) and 5(a)–5(d). [When the motion is locked, the torus is still present, but it is not visible because all points are attracted to the locked solution.] The torus changes shape and starts to break up as $\kappa\tau$ is increased further, up until the dynamics become chaotic [Figs. 4(e) and 4(f) and 5(e) and 5(f)]. The chaos suddenly stops with the appearance of a stable limit cycle ($\kappa\tau = 4.147$), which marks the end of bubble 2 [Figs. 4(g) and 4(h) and 5(g) and 5(h)]. This bifurcation is maybe even more stunning if we consider decreasing $\kappa\tau$ from 4.147 to 4.145: practically without any warning the dynamics change from periodicity to chaos. For a detailed description of this bifurcation see Sec. VI. We finally remark that all attractors in bubble 2 are symmetric.

D. Transition through bubble 3

The transition through bubble 3 can be found in Fig. 6 and the associated attractors of the Poincaré map are in Fig. 7; compare also Fig. 1(c). First, the symmetric limit cycle in Figs. 4(h) and 5(h) becomes unstable and two nonsymmetric limit cycles appear, one of which is shown in Figs. 6(a) and 5(a). As a consequence of this symmetry-breaking bifurcation, the power develops an extra maximum per period. In other words, we have identified the transition at $\kappa\tau \approx 4.7$ as a symmetry breaking bifurcation. It is *not* period doubling as one might surmise by studying only the bifurcation diagram; see also Sec. V.

The Poincaré map then undergoes a Hopf bifurcation which results in the appearance of a torus. The motion on the torus can be quasiperiodic or locked [Figs. 6(b) and 6(c) and 7(b) and 7(c)]. The torus breaks up and becomes chaotic for a large range of $\kappa\tau$ [Figs. 6(d) and 7(d)]. For $\kappa\tau = 6.45$ a torus reemerges, but it is very folded [Figs. 6(e) and 7(e)]. That we are indeed dealing with a torus becomes clear by considering the enlargement in Fig. 8 of the attractor of the Poincaré map in Fig. 7(e): it shows a very folded, but closed

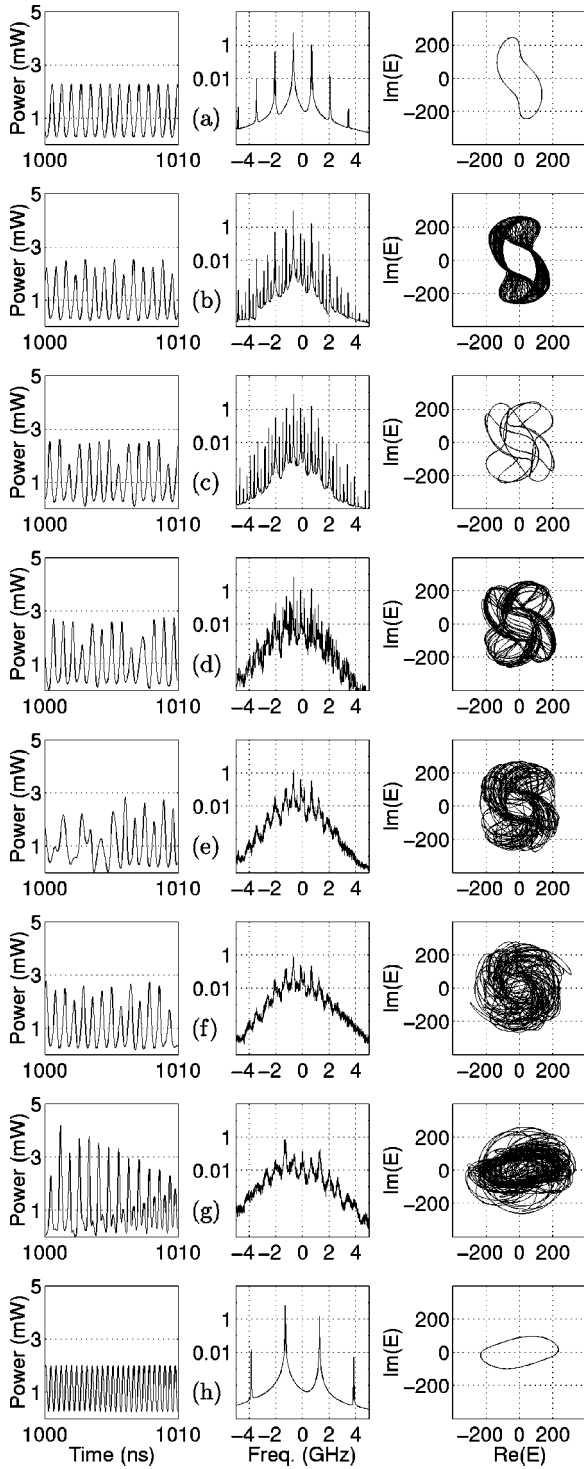


FIG. 4. Transition through bubble 2, showing the time series of the power (left panel), the optical spectrum (middle panel), and the trajectory in the E plane (right panel). From (a) to (h) $\kappa\tau = 2.2, 2.3, 2.45, 2.51, 2.55, 2.6, 4.145,$ and 4.147 .

curve. The torus gradually unfolds and becomes smoother [Figs. 6(f) and 7(f)], with occasional bursts into chaos; compare Fig. 1(c). Finally there is a Hopf bifurcation, the torus disappears, and we are left with a nonsymmetric limit cycle [Figs. 6(g) and 7(g)]. At $\kappa\tau \approx 6.65$ there is a symmetry-restoring bifurcation after which we are left with a symmetric limit cycle [Figs. 6(h) and 7(h)].

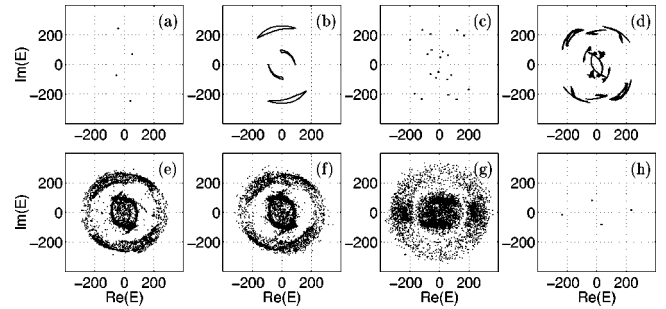


FIG. 5. Attractors of the Poincaré map of the transition through bubble 2 for the values of $\kappa\tau$ in Fig. 4.

V. CONSEQUENCES OF THE SYMMETRY

A change of the symmetry property of an attractor has important physical implications that are observable experimentally. Furthermore, the possibility of symmetry-breaking and -restoring bifurcations fundamentally distinguishes a laser with PCF from a laser with conventional optical feedback. In the latter case the system is symmetric under any rotation of the complex electric field [23], and consequently the bifurcations discussed here cannot occur there. It is surprising that this has not been observed earlier.

Let us consider what happens when a symmetric periodic orbit loses its stability and creates two symmetric stable limit cycles. This happens in the transition from Fig. 4(h) to Fig. 6(a) when $\kappa\tau$ is increased through ≈ 4.7 and also in the transition from Fig. 6(h) to 6(g) when $\kappa\tau$ is decreased through ≈ 6.65 . Suppose the symmetric limit cycle has the period T , so that it is of the form $\{(E(t), N(t)) | t \in [0, T)\}$. Notice that rotating the limit cycle by π around the N axis is equivalent with waiting for time $T/2$. Mathematically this means that

$$(-E(t-T/2), N(t)) = (E(t), N(t)) \quad \text{for all } t \in [0, T),$$

which implies that the time series of the power is periodic with period $T/2$; see Figs. 4(h) and 6(g). In other words, the frequency of the power is twice that of the limit cycle. When symmetry breaking occurs, this property is lost and the time series of the power is now periodic with period T , instead of $T/2$. Eventually the power will develop an extra maximum per period; see Figs. 6(a) and 6(g). This creates new intersection points that show up in the bifurcation diagram in Figs. 1(c). In other words, this symmetry breaking may be mistaken for a period doubling.

In the optical spectrum one notices the appearance of extra peaks at frequency $1/T$. But there is also another feature in the optical spectra, which allows one to distinguish symmetry breaking from period doubling. When the limit cycle is not symmetric there is an extremely narrow peak at the center of the optical spectrum [Figs. 6(a) and 6(g)]. This narrow peak is dominant when the phase of the laser is bounded, which means that the projection of the limit cycle does not surround the origin of the E plane. In other words, the laser phase no longer visits the entire range of 0 to 2π , and then the linewidth is significantly narrowed. This peak becomes smaller the more symmetric the limit cycle be-

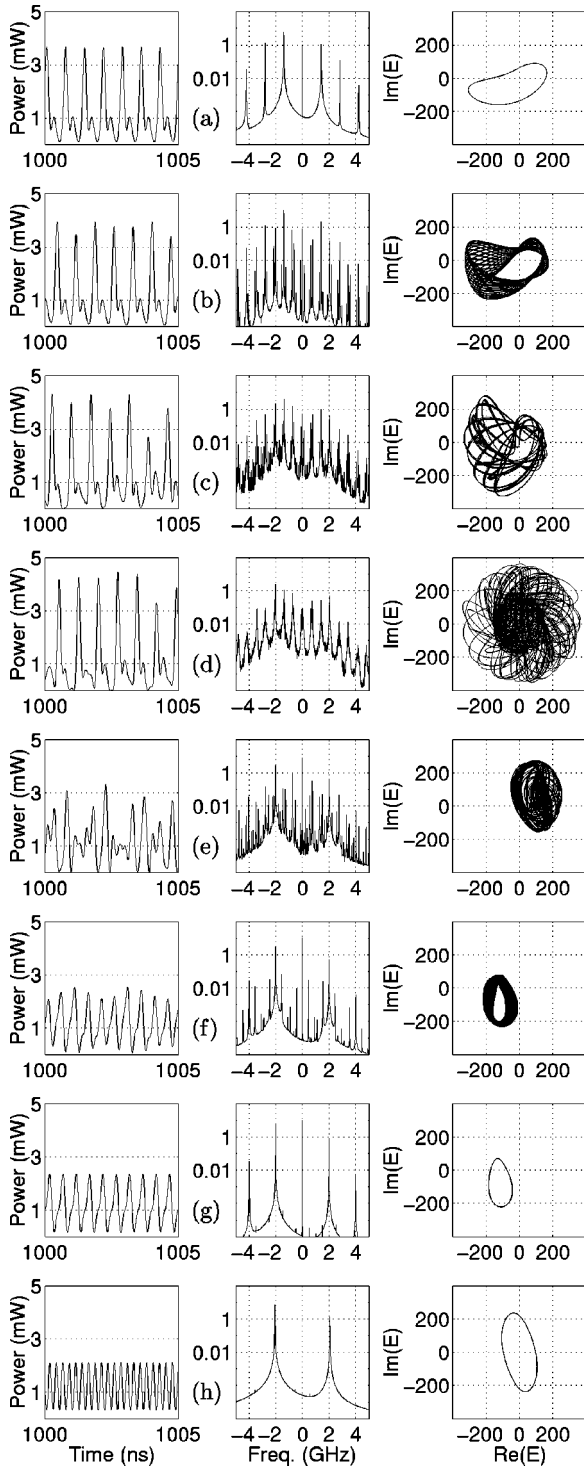


FIG. 6. Transition through bubble 3, showing the time series of the power (left panel), the optical spectrum (middle panel), and the trajectory in the E plane (right panel). From (a) to (h) $\kappa\tau = 5.0, 5.1, 5.47, 5.6, 6.45, 6.58, 6.6,$ and 6.7 .

comes. Indeed, when symmetry restoration occurs, as in Figs. 4(h) and 6(h), then the narrow central peak disappears.

This appearance and disappearance of the central peak is also present in the symmetry restoration involving a chaotic attractor in Figs. 2(c) and 2(d). Note that the phase is bounded for $\kappa\tau=0.79$, even though the dynamics is chaotic. When $\kappa\tau=0.8$ the dynamics is still chaotic, but the phase is no longer bounded, because the chaotic attractor has merged

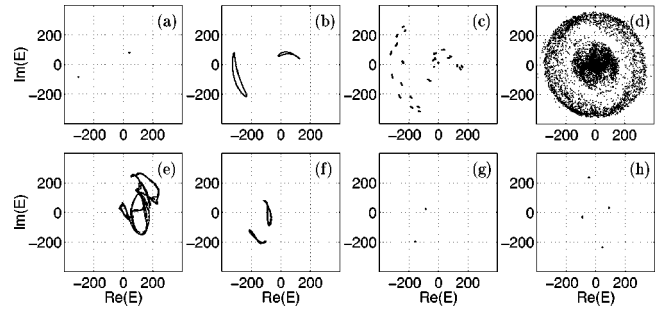


FIG. 7. Attractors of the Poincaré map of the transition through bubble 3 for the values of $\kappa\tau$ in Fig. 6.

with its symmetric counterpart. This leads to the disappearance of the central peak in the optical spectrum as was just discussed. Note that the change in the phase dynamics cannot be detected by just looking at the time series of the power, because the two halves of the attractor that are visited chaotically are symmetric images of each other.

VI. GLOBAL SADDLE-NODE BIFURCATION OF LIMIT CYCLES

At the end of bubble 2 there is no hysteresis: the laser jumps directly from chaos to stable oscillations as $\kappa\tau$ is increased through ≈ 4.146 , and it jumps from stable oscillations to full-scale chaos as $\kappa\tau$ is decreased through ≈ 4.146 , both virtually without warning [Figs. 4(g) and 4(h) and 5(g) and 5(h)]. This transition is a saddle-node bifurcation of limit cycles, where the unstable piece of the (two-dimensional) center manifold intersects the stable piece of the center manifold. This global aspect of this bifurcation is known to create complicated dynamics instantly, when the stable limit cycle collides with an unstable limit cycle and disappears [24,25]. There are several cases of complicated dynamics, like a suspension of a solenoid, or so-called random dynamics [25].

Here we show that indeed a saddle-node bifurcation of limit cycles is the bifurcation at hand. The question of which of the different cases of global dynamics occurs is beyond the scope of this paper. The fact that we are dealing with a saddle-node bifurcation of limit cycles is confirmed in Fig. 9, which shows an enlargement of the bifurcation diagram around $\kappa\tau=4.14$. One notices that the curve of stable limit

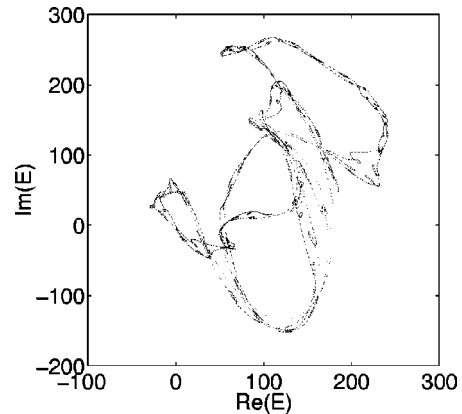


FIG. 8. Enlarging Fig. 6(e) ($\kappa\tau=6.45$) shows that this attractor of the Poincaré map is a closed curve with many self-intersections.

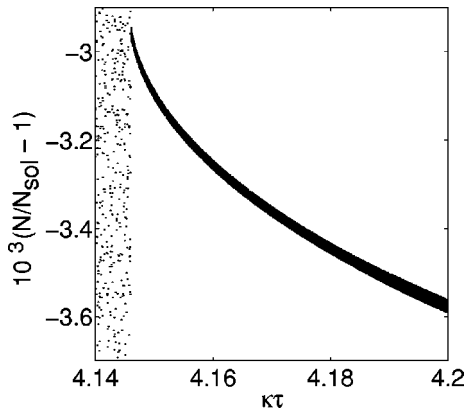


FIG. 9. Enlargement of the bifurcation diagram near the end of bubble 2. The curve of stable limit cycles appears as a parabola, which is typical for a saddle-node bifurcation of limit cycles.

cycles is a parabola that is tangent to the region of chaotic dynamics. This is a tell-tale sign of a saddle-node bifurcation of limit cycles [20]. More evidence is given by the fact that the “ghost” of the limit cycle that is about to appear is already present for $\kappa\tau=4.145$ [Figs. 4(g)]. The laser wants to settle down to the almost stable limit cycle, but then makes long chaotic excursions, which is an example of intermittency. This effect is shown more dramatically in Fig. 10 with a time series of the power for $\kappa\tau=4.145\,669\,3$. Notice several longer intervals where the dynamics is close to the ghost of the limit cycle before it drifts off again [Fig. 10(a)]. The longest such interval is enlarged in Fig. 10(b), and it should be compared with the time series in Fig. 4(h).

VII. CONCLUSIONS

The PCF laser shows a wealth of dynamical behavior. We believe that we have discovered most, if not all, of the dynamics and bifurcations in the PCF laser, at least up to feedback levels consistent with the assumption of weak PCF. Most prominent are periodic orbits, motion on a torus, and chaos. We find the well-known transitions to chaos via period doublings at the beginning of bubble 1, but most common is the transition via the breaking up of a torus. Most surprising is the immediate transition from a stable limit cycle to chaos at the end of bubble 2, which we identified as a global saddle-node bifurcation of limit cycles.

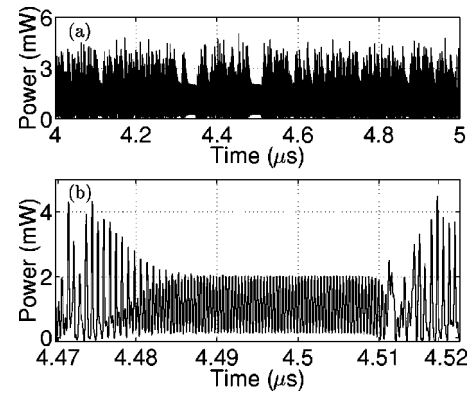


FIG. 10. Time series of the power for $\kappa\tau=4.145\,669\,3$ showing intervals where the dynamics is near the “ghost” of the limit cycle that is about to appear (a), and an enlargement of the largest such interval (b).

An important feature is the symmetry of the system under π phase changes. This leads to attractors that are either symmetric or that have symmetric counterparts. We found several examples of symmetry-breaking and -restoring bifurcations. The optical spectrum turns out to be useful for predicting whether the system has settled on a symmetric or a nonsymmetric attractor. This is because when the attractor is nonsymmetric, then the laser phase tends to be bounded, which leads to a narrowing of the low frequency part of the optical spectrum.

The dynamics and their bifurcations are only hinted at by a bifurcation diagram, even if it is as detailed as in Fig. 1. We have argued that a detailed analysis in phase space is needed to completely describe the dynamics. This is also true for other systems, such as the laser with conventional optical feedback from a regular mirror.

ACKNOWLEDGMENTS

The authors thank J. Guckenheimer and Yu. Ilyashenko for helpful comments on the global saddle-node bifurcation of limit cycles, and The Geometry Center, University of Minnesota, for its hospitality and support. This work was partially supported by NATO under Collaborative Research Grant No. CRG 941327. The research of B.K. was supported by the Foundation for Fundamental Research on Matter (FOM), which is financially supported by The Netherlands Organization for Scientific Research (NWO).

-
- [1] G. R. Gray, D. H. DeTienne, and G. P. Agrawal, *Opt. Lett.* **20**, 1295 (1995).
 - [2] G. H. M. van Tartwijk, H. J. C. van der Linden, and D. Lenstra, *Opt. Lett.* **17**, 1590 (1992).
 - [3] G. P. Agrawal and G. R. Gray, *Phys. Rev. A* **46**, 5890 (1992).
 - [4] G. R. Gray, D. Huang, and G. P. Agrawal, *Phys. Rev. A* **49**, 2096 (1994).
 - [5] N. Cyr, M. Breton, M. Tetu, and S. Theriault, *Opt. Lett.* **16**, 1298 (1991).
 - [6] T. Shimura, M. Tamura, and K. Kuroda, *Opt. Lett.* **18**, 1645 (1993).
 - [7] S. Maillhot and N. McCarthy, *Can. J. Phys.* **71**, 429 (1993).
 - [8] G. P. Agrawal and J. T. Klaus, *Opt. Lett.* **16**, 1325 (1991).
 - [9] G. H. M. van Tartwijk and D. Lenstra, *Quantum Semiclass. Opt.* **7**, 87 (1995).
 - [10] D. H. DeTienne, G. R. Gray, G. P. Agrawal, and D. Lenstra, *Proc. SPIE* **2693**, 689 (1996).
 - [11] D. H. DeTienne, G. R. Gray, G. P. Agrawal, and D. Lenstra, *IEEE J. Quantum Electron.* **33**, 838 (1997).
 - [12] W. A. van der Graaf, L. Pesquera, and D. Lenstra, *Opt. Lett.* **23**, 256 (1998).
 - [13] W.A. van der Graaf, L. Pesquera, and D. Lenstra, *Proc. SPIE* **3283**, 522 (1988).
 - [14] M. W. Pan, B. P. Shi, and G. R. Gray, *Opt. Lett.* **22**, 166 (1997).
 - [15] J. Hale and S. M. Verduyn Lunel, *Functional Differential*

- Equations*, Applied Mathematical Sciences Vol. 99 (Springer, Berlin, 1993).
- [16] O. Diekmann, S. A. van Gils, S. M. V. Lunel, and H.-O. Walther, *Delay Equations*, Applied Mathematical Sciences Vol. 110 (Springer, Berlin, 1995).
- [17] M. Golubitsky and D.G. Schaeffer, *Singularities and Groups in Bifurcation Theory I*, Applied Mathematical Sciences Vol. 51 (Springer, Berlin, 1985).
- [18] M. Golubitsky, I. Stuart, and D. G. Schaeffer, *Singularities and Groups in Bifurcation Theory II*, Applied Mathematical Sciences Vol. 69 (Springer, Berlin, 1988).
- [19] J. Guckenheimer and P. Holmes, *Nonlinear Oscillations, Dynamical Systems and Bifurcations of Vector Fields*, 2nd ed., Applied Mathematical Sciences Vol. 42 (Springer, Berlin, 1986).
- [20] Yu. Kuznetsov, *Elements of Applied Bifurcation Theory*, Applied Mathematical Sciences Vol. 112 (Springer, Berlin, 1995).
- [21] B. Krauskopf, G. R. Gray, and D. Lenstra, Proc. SPIE **3283**, 510 (1998).
- [22] B. Krauskopf, G. R. Gray, and D. Lenstra, VUTH-eprint 98-13, available at <http://www.nat.vu.nl/vakgroepen/theorie/english/publications/eprints/vuth98-13/vuth98-13.html>
- [23] B. Krauskopf and G. H. M. van Tartwijk, VUTH-eprint 98-15, available at <http://www.nat.vu.nl/vakgroepen/theorie/english/publications/eprints/vuth98-15/vuth98-15.html>
- [24] D. Turaev, Int. J. Bifurcation Chaos Appl. Sci. Eng. **6**, 919 (1996).
- [25] Yu. Ilyashenko and Li Weigu, *Nonlocal Bifurcations* (American Mathematical Society, Providence, in press).